

# X-rays associated with the jet-cloud interacting radio galaxy 3C 277.3 (Coma A): implications for energy deposition

D.M. Worrall<sup>1,2</sup>, M. Birkinshaw<sup>1,2</sup> and A.J. Young<sup>1</sup>

<sup>1</sup>*HH Wills Physics Laboratory, University of Bristol, Tyndall Avenue, Bristol BS8 1TL*

<sup>2</sup>*Harvard-Smithsonian Center for Astrophysics, 60 Garden Street, Cambridge, MA 02138, USA*

2 February 2016

## ABSTRACT

We report the discovery with *Chandra* of X-ray-emitting gas associated with the jet-cloud interaction in the radio galaxy 3C 277.3 (Coma A), a source that falls in the most important power range for radio-mode feedback in the Universe. This hot gas, heated by the jet, dominates the mass of the cloud which is responsible for an extreme projected deflection of the kpc-scale radio jet. Highly absorbed X-ray emission from the nucleus of 3C 277.3 confirms that the jet lies close to the plane of the sky and so has a large intrinsic deflection. We detect group gas on the scale of the radio lobes, and see X-ray cavities coincident with the brightest radio emission, with the lobes embraced by X-ray enhancements that we argue are the result of shocks. The anti-correlation between the locations of X-ray arms and H $\alpha$ -emitting filaments that are believed to have originated from a merger with one or more gas-rich galaxies suggests that shocks advancing around the lobe are inhibited by the dense colder material. Synchrotron X-ray emission is detected from the upstream edge of a second bright radio knot. X-rays are also detected from the location where an undetected counterjet enters the northern radio hotspot. We suggest that these X-rays are synchrotron radiation from a shock in a small-scale substructure.

**Key words:** galaxies: active – galaxies: jets – galaxies: individual: (3C 277.3, Coma A) – galaxies: ISM – radio continuum: galaxies – X-rays: galaxies

## 1 INTRODUCTION

The persistence of radio galaxies means that the sources must be expanding into an external medium. X-ray-emitting plasma held in the potential wells of galaxies, groups, and clusters dominates that medium. Dynamical studies are hampered both by the fact that radio-source emission is predominantly non-thermal, and by instrumentation that cannot yet provide the spatially-resolved high-resolution X-ray spectroscopy needed to probe the dynamics of the X-ray gas through its line emission. If the X-ray gas is mixed with cooler ionized material that emits lines in the optical or near infrared, or neutral gas emitting in the radio or sub-mm, then dynamical studies are greatly enhanced. For this reason, the study of radio galaxies with cooler emission-line gas in their environments is of particular interest, especially those displaying jet-cloud interactions, where an interaction interface is directly revealed. A prominent case previously unstudied in X-rays is 3C 277.3 (Coma A).

There is an additional reason that 3C 277.3 is impor-

tant: its radio power and morphology place it on the borderline between the FRI and FRII classes. Radio galaxies are recognized as the primary sources for the energy needed to maintain cluster cores, and for playing a dominant rôle in the self-regulated feedback loop between black-hole and galaxy growth (McNamara & Nulsen 2012). An understanding of how radio-mode feedback actually works remains incomplete, and is based primarily on observations of radio sources that are nearest and most abundant, and hence members of the FRI population. The scaling of cavity and radio power that is found (Cavagnolo et al. 2010), when combined with the radio luminosity function (Best et al. 2005), means that radio-mode feedback is dominated by sources of FRI/II transition power (Worrall 2009), with half the total heating expected from sources with powers 0.3 – 3 times the FRI/II transition power. Interestingly the jet-cloud interacting radio source PKS B2152-699 is also of FRI/II transition power. PKS B2152-699 has been the subject of in-depth study with *Chandra* (Ly, De Young & Bechtold 2005;

Young et al. 2005; Worrall et al. 2012), and makes an interesting comparison case for 3C 277.3.

3C 277.3 is a relatively small double-lobed radio galaxy (total size about 65 kpc), studied in detail by van Breugel et al. (1985). In the northern lobe there is a prominent hotspot but no obvious jet, whereas in the southern lobe two radio knots delineate a dramatic bend in the jet through a projected angle of about  $40^\circ$ , but there is no hotspot. While also known as Coma A, 3C 277.3 lies behind the Coma cluster and is offset from its centre by about 75 arcmin, outside the boundary of cluster X-ray emission.

The entire 3C 277.3 system is rich in cool gas emitting in a number of optical lines (van Breugel et al. 1985) and cold hydrogen is seen in absorption at 21 cm (Morganti et al. 2002). The H $\alpha$  emission-line gas forms a system of large-scale arcs and filaments which extend almost as far perpendicular as parallel to the radio axis, and which appear to bound the radio lobes (Tadhunter et al. 2000). What is exciting this gas is uncertain, and while Tadhunter et al. (2000) favour shocks as being dominant, they do not rule out photoionization from young stars in the filaments. The observation of resolved HI absorption that is detected against both radio lobes with velocity structure matched to that seen in emission-line gas has led Morganti et al. (2002) to suggest that the ionized and neutral gas are two phases of the same structure, of total gas mass at least  $10^9 M_\odot$ , resulting from a merger of 3C 277.3's host with at least one large gas-rich galaxy. The cold gas is deduced to be filamentary on a sub-arcsec scale: an anti-correlation of radio polarization and H $\alpha$  emission, particularly in the northern hotspot and around the southern jet, is interpreted as the result of differential Faraday rotation from multiple clumps of thermal material lying within the radio beam (van Breugel et al. 1985; Baum & Heckman 1989). The general conclusion is that 3C 277.3 is expanding into a gas disk (Morganti et al. 2002).

3C 277.3's designation as a jet-cloud interacting radio galaxy is due to the bright optical emission-line knot that lies adjacent to the large bend in the southern jet, and with which the jet is interacting (van Breugel et al. 1985; Solórzano-Iñarrea & Tadhunter 2003; Tilak et al. 2005).

Balmaverde et al. (2012) comment on blobs of X-ray emission cospatial with two radio knots and the northern hotspot. However, the quality of the data was insufficient to locate the X-ray features accurately, address emission mechanisms, or search for faint diffuse emission. Here we discuss much improved *Chandra* X-ray data, revealing that the jet-cloud interaction region is dominated in mass by X-ray emitting gas, and that the system resides in a group atmosphere. We estimate the level of power injected by the radio source into the cloud and into the larger-scale group gas, thus addressing the heating of the external medium by a characteristic radio galaxy in a characteristic atmosphere, and so important for the Universe as a whole. The source is classified by its nuclear spectrum as a High Excitation Galaxy (HEG; Buttiglione et al. 2009, 2010), and we also report here on the X-ray emission from the nucleus, as well as that from the southern jet and northern hotspot. We adopt values for the cosmological parameters of  $H_0 = 70 \text{ km s}^{-1} \text{ Mpc}^{-1}$ ,  $\Omega_{m0} = 0.3$ , and  $\Omega_{\Lambda0} = 0.7$ . Thus 1 arcsec corresponds to a projected distance of 1.6 kpc at 3C 277.3, for its redshift of  $z = 0.0853$  (Rines et al. 2001).

## 2 OBSERVATIONS AND REDUCTION METHODS

### 2.1 *Chandra* X-ray

We observed 3C 277.3 in VFAINT full-frame data mode with the Advanced CCD Imaging Spectrometer (ACIS) on board *Chandra* in four exposures taken between 2014 March 11th and 16th (OBSIDs 15023, 15024, 16599, 16600). The source was positioned at the nominal aimpoint of the front-illuminated I3 chip. Our analysis combines these data with those from an archival ACIS exposure (OBSID 11391, Balmaverde et al. 2012) taken on 2010 March 3rd in the same data mode but with the source positioned at the nominal aimpoint of the back-illuminated S3 chip. Details of the ACIS instrument and its modes of operation can be found in the *Chandra* Proposers' Observatory Guide<sup>1</sup>. Results presented here use CIAO V4.7 and the CALDB V4.6.8 calibration database. We re-calibrated the data, with random pixelization removed, the energy-dependent sub-pixel event repositioning algorithm applied, and bad pixels masked, following the software 'threads' from the *Chandra* X-ray Center (CXC)<sup>2</sup>, to make new level 2 event files. Only events with grades 0,2,3,4,6 were used, as recommended.

The observations were free from background flares and, after removal of time intervals when the background deviated more than  $3\sigma$  from the average value, the total exposure time was 213 ks, distributed as follows: OBSID 15023, 43.114 ks; 15024, 19.828 ks; 16599, 28.513 ks; 16600, 96.744 ks; 11391, 24.770 ks. The astrometry was adjusted (by between 0.5 and 1 arcsec, mostly in RA) so that for each observation the X-ray core aligned with the radio-core position measured from our highest-resolution 4.9 GHz map (Section 2.2) of RA =  $12^{\text{h}}54^{\text{m}}11^{\text{s}}.993$ , Dec =  $27^\circ37'33''.87$ .

The CIAO WAVDETECT task was used to find sources in a merged 0.4–5-keV image of the 2014 data, with the threshold set at 1 spurious source per field. Except for those detections corresponding to features associated specifically with features of 3C 277.3, the corresponding regions were excluded from spectral analysis, and were refilled using DM-FILTH before making image figures. All spectral fitting includes absorption along the line of sight in our Galaxy assuming a column density of  $N_{\text{H}} = 0.72 \times 10^{20} \text{ cm}^{-2}$  [from the COLDEN program provided by the CXC, using data of Dickey & Lockman (1990)], including where models are described as unabsorbed.

Throughout the paper the power-law spectral index,  $\alpha$ , is defined in the sense that flux density is proportional to  $\nu^{-\alpha}$ . X-ray spectral indices are quoted in terms of  $\alpha$  rather than the values one larger returned by spectral-fitting codes. Uncertainties correspond to 90 per cent confidence, unless otherwise stated.

### 2.2 VLA radio

For this work we mapped VLA data from the programmes, arrays and frequencies given in Table 1. The data were calibrated, flagged for interference, and passed through the normal clean and gain self-calibration cycles in AIPS. Figure 1

<sup>1</sup> <http://cxc.harvard.edu/proposer>

<sup>2</sup> <http://cxc.harvard.edu/ciao>

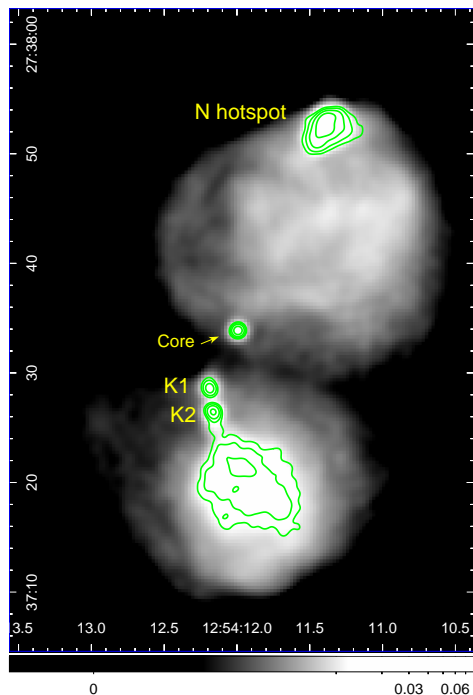


**Figure 1.** Radio structure of 3C 277.3. Image of 1.4-GHz data with 1.3-arcsec beam (entry 3 of Table 1) with scale bar in Jy, with contours from the 4.8-GHz data with 0.4-arcsec beam (entry 1 of Table 1) increasing by factors of 2 from the lowest contour at 0.2 mJy beam<sup>-1</sup>.

shows the overall structure and prominent components of the radio source. The source has well-rounded diffuse lobes, a prominent northern (N) hotspot, and two bright southern knots which are labelled K1 and K2, following [Bridle et al. \(1981\)](#).

### 3 RESULTS

#### 3.1 Overall X-ray characteristics

The five *Chandra* data sets were exposure corrected and combined to make the 0.4–5-keV combined image shown in Figure 2. Here X-rays associated with the core, two knots in the southern jet (K1, K2) and the N hotspot are readily apparent. Most pixels contain no counts.

The application of adaptive smoothing to the image in Figure 2 shows underlying diffuse structure (Fig. 3), whereas the background should be roughly uniform over the image. The X-rays show a rough morphological anti-correlation with the radio, with the X-rays appearing to embrace the radio lobes. Figure 3 shows X-ray cavities in the brightest parts of the S and N lobes (disregarding the N hotspot and S jet). The region directly to the SW of the core is faint in X-rays where the radio too is weak, but there is an apparent X-ray increase further out, bordering the faintest radio contour in the image. The X-ray structures are reminiscent of the arms seen in H $\alpha$  emission ([Tadhunter et al. 2000](#)), a point to which we will return in Section 4.1.

The alignment of the N hotspot, core and K1 in the radio (e.g., Fig 1) suggests that the southern radio jet enters

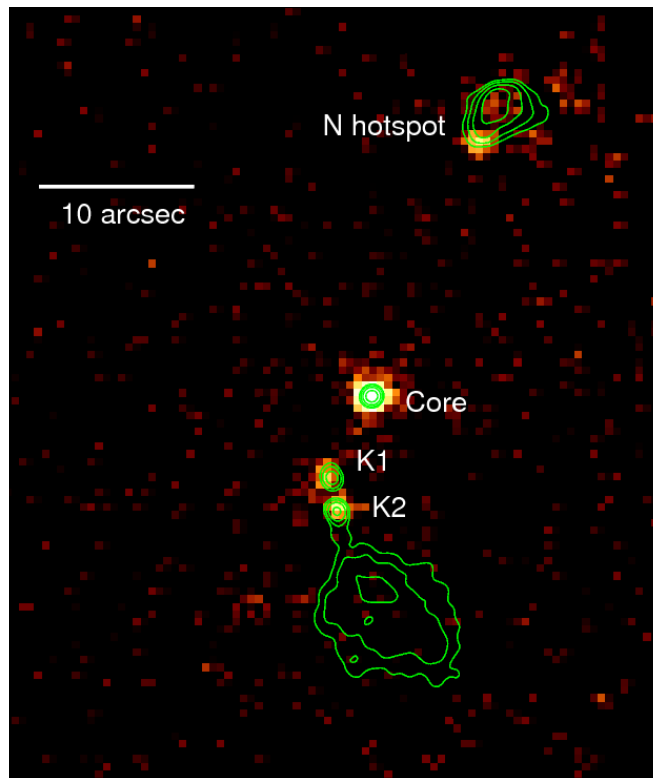


**Figure 2.** Exposure-corrected 0.4–5-keV *Chandra* image in 0.492 arcsec pixels. Radio contours are from Fig. 1.

K1 from the NW and deflects by a projected angle of almost 40 degrees to reach K2. The X-ray and radio data are registered on the core to better than 0.1 arcsec, rendering the offsets between the radio and X-ray in K1 and K2 (Fig. 4) striking. At K1 the X-rays are displaced at the outer edge of the radio bend, and better aligned with the optical emission-line gas discussed in Section 4.2. At K2 the X-rays are along the path of the radio jet, although peaked upstream of the radio knot.

There is X-ray emission covering the N hotspot, as clear from Figures 2 and 3. The brightest X-ray emission is at the upstream edge, where the counterjet is presumed to enter the hotspot (Fig. 5). While we cannot rule out a foreground or background source as responsible for these X-rays, our catalogue and image searches at other wavelengths, including the use of archival *HST* data, revealed no strong candidates for an identification. We note that the western X-ray extension of the N hotspot seen in Figure 3 is unreliable because here the exposure has dropped by a factor of two due to proximity to a CCD chip gap, allowing the exposure correction to emphasize a statistically small number of counts.

#### 3.2 Core

We have fitted the spectrum (roughly 1200 net counts 0.4–7 keV) extracted from a circle of radius 1.25 arcsec centered on the core, using local background, to various models. The data and calibrations for the 2014 observations were combined before fitting. Data were grouped to 15 counts/bin and the weighting scheme of [Churazov et al. \(1996\)](#) was

**Table 1.** *VLA/* Radio Data

(1) Programme	(2) Observation Date	(3) Frequency (GHz)	(4) Configuration	(5) Restoring Beam (arcsec) <sup>2</sup>	(6) Noise ( $\mu\text{Jy beam}^{-1}$ )
VANB <sup>a</sup>	1981 Mar 18	4.87	<i>VLA</i> A	$0.40 \times 0.37$	78
VANB <sup>a</sup>	1981 May 31	4.89	<i>VLA</i> B	$1.28 \times 1.22$	54
VANB <sup>a</sup>	1981 Mar 18	1.41	<i>VLA</i> A	$1.38 \times 1.34$	133
AB348	1985 Aug 26	14.94	<i>VLA</i> C	$1.53 \times 1.24$	111

*a.* Data originally published in [van Breugel et al. \(1985\)](#)

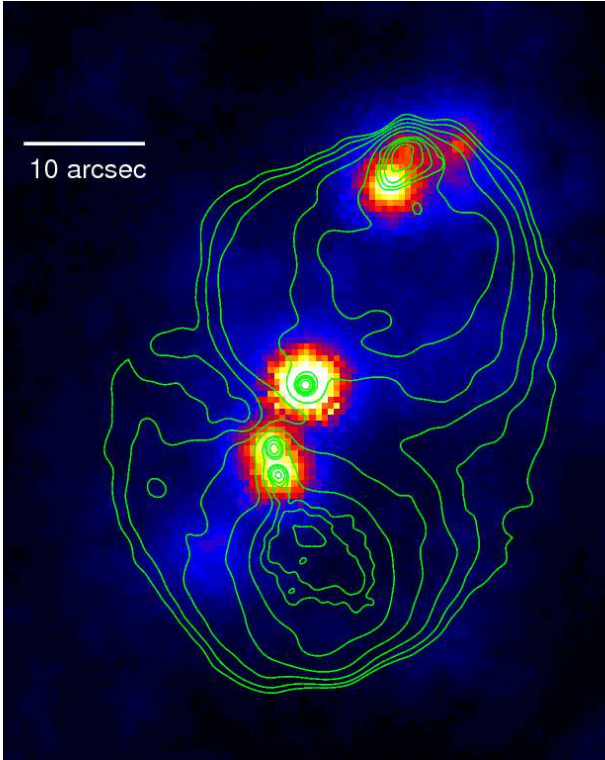


**Figure 3.** Adaptively-smoothed exposure-corrected 0.4–5 keV *Chandra* image together with both the radio contours of Fig. 1 and those from the 1.4-GHz data with 1.3-arcsec beam (entry 3 of Table 1) increasing by factors of 2 from the lowest contour at  $0.4 \text{ mJy beam}^{-1}$ .

adopted to provide an improved estimate of the variance in the limit of small numbers of counts. While a single-component power-law model gave a bad fit, it was noticeable that the spectral index was abnormally hard,  $\Gamma \approx 0$  (i.e., flux-density rising with energy:  $\alpha_x \approx -1$ ), and there was structure in the residuals, with a broad deficiency of counts between about 2 and 3 keV and excess counts at high and low energies. This suggested the presence of an additional component that is heavily absorbed. The distribution of spectral counts did not agree with that normal for nearby FRI radio galaxies: a weakly absorbed power law, possibly mixed with a small component of thermal emission from central gas (e.g., [Evans et al. 2006](#)). The spectral index for the heavily absorbed component was not well constrained, and when fixed at  $\Gamma = 1.7$  ( $\alpha_x = 0.7$ ) the excess absorption over the Galactic value was characterized by an  $N_H$  of about  $3 \times 10^{23} \text{ cm}^{-2}$ . A problem remained in that the

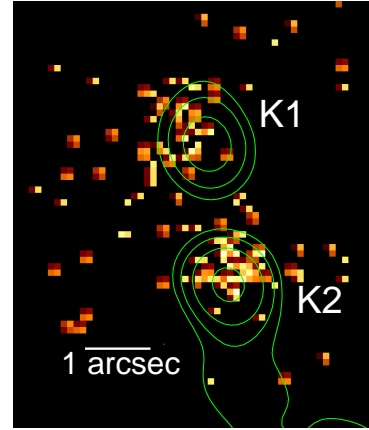


**Figure 4.** Same as Figure 2 but zoomed to show the K1–K2 region in more detail, and with the X-ray mapped into sub pixels of 1/5th the native size (i.e., 0.0984 arcsec). Relative to the radio, the X-ray emission is displaced on the outer edge of the bend at K1 and upstream where the jet flows into K2.

component of unabsorbed emission remained unphysically inverted, at  $\alpha_x \approx -1$ .

We found that fits were unacceptable unless the normalization of the highly-absorbed emission (that dominates above about 3 keV) decreased between the 2010 and 2014 observations. Variability was not required for the unabsorbed component whose parameters were linked between the data sets. This model of a very hard, unabsorbed, low-energy component ( $\alpha_x = -1.2$ ) plus a component of typical (fixed) spectral index and high absorption, gave an acceptable fit of  $\chi^2 = 85.5$  for 70 degrees of freedom. Of course we cannot be sure it is the emission that has decreased and not the absorption that has increased, or at least some combination of the two. But, the alternative of keeping a fixed normalization and fitting  $N_H$  as 1.9 and  $3.6 \times 10^{23} \text{ cm}^{-2}$  in 2011 and 2014, respectively, gave a somewhat worse fit of  $\chi^2 = 91.2$  for 70 degrees of freedom, and allowing both normalization and  $N_H$  to be free parameters found the solution where only the normalization varied.

While the model above explains some characteristics of the core emission, it does not explain the unphysically hard spectral index found for the unabsorbed, non-variable, emission. We thus investigated changing the absorption model from the simplest case of a single column density. A partial covering model applied to a single-component power law of  $\alpha_x > 0$  did not give a good fit, even if the normalization and the parameters of the absorption were allowed to vary between 2010 and 2014 (e.g.,  $\chi^2 = 188.5$  for 69 degrees of



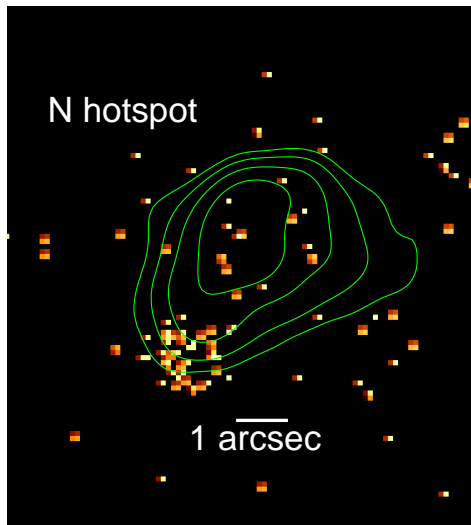


**Figure 5.** Same as Figure 4 but for the N hotspot, showing that the X-rays are bright at the upstream edge, where the jet presumably enters.

freedom with  $\alpha_x = 0.7$ ). However, a power-law distribution of column densities ranging from  $10^{15}$  to  $10^{24}$   $\text{cm}^{-2}$  (fixed), with the covering factor independent of column density i.e., the model of Done & Magdziarz (1998) with  $\beta = 0$ , produces a marginally acceptable fit of  $\chi^2 = 94.0$  for 72 degrees of freedom for a fitted power-law index of  $\alpha_x = 0.69^{+0.12}_{-0.13}$ , and  $\chi^2$  reduces by 3 for one extra parameter if about 0.2 per cent of the 1-keV flux density is unabsorbed (Fig. 6). For this model the 1-keV flux density of the absorbed emission (after correction for absorption) dropped from about 230 nJy in 2010 to 150 nJy in 2014. The data quality is insufficient for us to comment reliably on the possible presence of a 6.4-keV Fe line. The 0.5–7 (2–10)-keV core power (corrected for absorption) was  $3(2.5) \times 10^{43}$  and  $2(1.7) \times 10^{43}$   $\text{ergs s}^{-1}$  in 2010 and 2014, respectively. The 1-keV flux density in the component which is unabsorbed is only about 0.3 nJy.

While the details of the absorption are likely to be complex and cannot be uniquely determined by these data, we conclude that the overall core emission decreased significantly in strength between 2010 and 2014, and the material covering the source is non-uniform, reaching a maximum column density as high as about  $10^{24}$   $\text{cm}^{-2}$ . 3C 277.3's nuclear emission-line classification is that of HEG, and like all HEG in the low-redshift 3CR sample, shows morphology that is predominantly FR II (Buttiglione et al. 2010). Following Evans et al. (2006), the nuclear X-ray emission of such galaxies is usually dominated by emission which is absorbed by  $N_H > 10^{23}$   $\text{cm}^{-2}$  and which is supposed to arise from structures associated with the accretion flow, with a smaller contribution from unabsorbed emission assumed to be jet related in origin. 3C 277.3 appears to validate such a picture. The X-ray luminosity (corrected for absorption) is lower than that of a typical FR II in Evans et al. (2006), pointing to a less luminous accretion flow, as might be anticipated for a source of intermediate FRI/II power.

Morganti et al. (2002) find no HI in absorption against the radio nucleus. Given the X-ray absorption results, the logical conclusion is that the radio jet becomes bright only

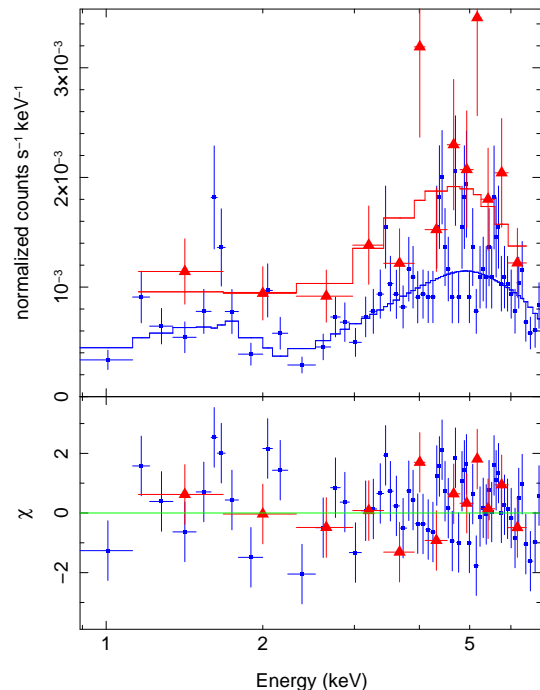


**Figure 6.** Core spectrum fitted to a power-law model absorbed by a power-law distribution of column densities, as described in the text. The red triangles and upper model curve correspond to the 2010 ACIS-S data, and the blue squares and lower curve to the 2014 ACIS-I data. The lower panel shows residuals expressed as their individual contributions,  $\chi$ , to  $\chi^2$ .

after it has penetrated the environment of the absorbing gas. The flat radio spectrum (e.g.,  $\alpha_r \approx 0.1$  between 1.4 and 5 GHz in 1981) shows it is still moderately synchrotron self-absorbed at that point. The geometry of the absorbing gas is unknown, but radio-galaxy jets passing through the holes of a toroidal structure whose axis is in the plane of the sky is the picture generally adopted by unified models (e.g., Urry & Padovani 1995) to explain the existence of beamed sources with no central X-ray or optical absorption. With 3C 277.3, we have perhaps the most convincing evidence in a relatively powerful radio galaxy that the nuclear X-ray emission is dominated by a variable sub-pc component on a scale smaller than that at which the inner radio jets become bright. Within the context of unified models, the high inner absorption argues that the source is relatively close to the plane of the sky.

Considering now the base of the radio jet, we should attribute to it only the non-varying core X-ray component that is entirely unabsorbed (0.3 nJy at 1 keV). By comparison, our highest-resolution radio map reveals the core 5-GHz flux density to have been 12.4 mJy in 1981 (Table 2). The interpolated radio to X-ray spectral index is then  $\alpha_{rx} \approx 1$  for the base of the jet. If we include data for the optical nucleus measured by Capetti et al. (2002) and interpreted as synchrotron radiation,  $\alpha_{ro} \approx 0.75$  and  $\alpha_{ox} \approx 1.4$ .

### 3.3 N hotspot

The spectrum of the bright upstream edge of the N hotspot was extracted from a circle of radius 2 arcsec. Local back-

**Table 2.** Parameters for radio components

(1) Component	(2) RA, Dec	(3) $S_{1.4 \text{ GHz}}$ (mJy)	(4) $S_{4.9 \text{ GHz}}$ (mJy)	(5) FWHM (arcsec)	(6) PA (deg)	(7) $\alpha_r$
Core	12:54:11.999 $\pm$ 0.007, 27:37:33.91 $\pm$ 0.06	14.2 $\pm$ 0.2	12.4 $\pm$ 0.2	–	–	0.11 $\pm$ 0.02
K1	12:54:12.190 $\pm$ 0.005, 27:37:28.64 $\pm$ 0.05	16.2 $\pm$ 0.6	7.1 $\pm$ 0.2	0.7 $\times$ 0.3	21	0.67 $\pm$ 0.04
K2	12:54:12.174 $\pm$ 0.003, 27:37:26.30 $\pm$ 0.08	26.5 $\pm$ 0.6	11.6 $\pm$ 0.3	0.6 $\times$ 0.4	32	0.67 $\pm$ 0.04

1 $\sigma$  errors.

ground was measured from a source-centered half annulus of radii 2.5 to 10 arcsec to the SE, completely on the same CCD chip as the hotspot (I3 and S3 for the 2014 and 2011 data, respectively). There are only about 40 net counts in the band 0.4–7 keV, and so they were fitted using the Cash statistic (cstat within XSPEC) using a power-law model, to find a spectral index of  $\alpha_x = 1.3^{+0.8}_{-0.7}$  and 1-keV flux density of  $0.7^{+0.4}_{-0.3}$  nJy. Results are very similar using  $\chi^2$  and Churazov weighting with 5 counts per bin. If fitted to a thermal (apec) model,  $kT$  is hot, at about 3 keV, which does not suggest any obvious type of physical object. Nonthermal emission is far more likely.

### 3.4 K1 and K2

The spectral-fitting approach for K1 and K2 was similar to that for the N hotspot, except that polygons were used. Net counts for the both regions agree within statistics with one another and with the N hotspot.

Results for K2 are similar to those for the N hotspot, with a thermal fit giving a high  $kT$  (about 3.8 keV, and an abundance value that tends to zero), while a power-law fit gives a result that is understandable in the context of X-ray jet knots in other sources, finding  $\alpha_x = 1.0 \pm 0.6$  with a 1-keV flux density of  $0.4^{+0.2}_{-0.1}$  nJy. We interpret these X-rays as being nonthermal in nature.

However, the contrary is true for K1. A power-law spectral fit gives an abnormally steep spectral index of  $\alpha_x = 3.2 \pm 1.1$ , whereas a thermal fit gives reasonable parameter values. The abundance is poorly constrained at  $< 1.0$  and  $kT = 0.37^{+0.7}_{-0.1}$  keV.

Table 2 gives details of the radio emission from K1 and K2. Similar to the inner jet/core (see above), the interpolated radio (5 GHz) to X-ray spectral index for K2 is  $\alpha_{rx} \approx 1$ . K1 is fainter than K2 in the radio, and while we cannot rule out some of the X-rays seen in this region as having a non-thermal origin, the X-ray spectral data combined with the closer morphological association of the X-rays to emission-line gas in the jet deflection region (Section 4.2) than to the radio, lead us to consider only a thermal origin for the K1 X-rays.

### 3.5 Large-scale X-ray emission

We have used an ellipse of semi-major and semi-minor axes 28.5 and 22.3 arcsec, respectively, enclosing the radio source, to sample the spectrum of the large-scale gas. The background was measured from larger source-free regions on the relevant I3 or S3 chips. Regions covering K1, K2, the N hotspot, the core (a circle of generous radius 5 arcsec

to exclude the wings of the point spread function), and other sources found by WAVDETECT are excluded. The fit to a single-temperature thermal (APEC) model is acceptable ( $\chi^2 = 12.5$  for 14 degrees of freedom). The temperature,  $kT = 1.0 \pm 0.3$  keV, is compatible with a weak group atmosphere, although uncertainties are large.

We checked our procedure using background measured from the *Chandra* blank-sky fields. We followed the method we used in Worrall & Birkinshaw (2014), where we found the normalization correction needed to match source and background fields at 9.5–12-keV (where particle background dominates) was less than 3%. While the same was true here for the ACIS-S data, to match the 2014 ACIS-I data we needed to reduce the level of the sky-background data by the large factor of 30%, perhaps as a result of the 2014 observation being made close to Solar Maximum, when particle background is reduced. Although the large correction factor questions the appropriateness of the sky-background files for the ACIS-I observations here, we note that our spectral results were in excellent agreement with those from local background, in finding  $kT = 1.0 \pm 0.3$  keV.

The abundances found in our fits were low, at  $0.05^{+0.10}_{-0.04}$  times solar, but this may be an artifact of fitting a simple model to a region which is likely to include temperature structure, together with contributions from unresolved low-mass X-ray binaries and X-rays arising from inverse Compton scattering of the Cosmic Microwave Background radiation (iC-CMB) by an electron population responsible for the radio synchrotron emission, as detected in many lobed radio galaxies (e.g., Croston et al. 2005).

We argue that in 3C 277.3 emission from diffuse thermal gas *dominates* the extended X-rays. Firstly, X-ray binaries are estimated at only a few per cent of the 1-keV flux density based on typical integrated luminosities in elliptical galaxies taken from Kim & Fabbiano (2004). A more important consideration is iC-CMB emission. This should be strongest where the radio is brightest. While to some degree that is true, in that the extent of X-ray emission evident in Figure 3 is similar to that of the overall radio source, there is a greater association with the surrounds of the lobes than with regions where the lobes are radio brightest (see Section 3.1).

For a more quantitative assessment of the iC-CMB emission we first note that it is difficult spectrally over the *Chandra* bandpass to discriminate between gas of temperature roughly 1 keV and steep-spectrum power-law emission unless statistics are very good. The difficulty applies here, and a fit to a single-component power law is formally acceptable, but the spectral index of  $\alpha_x = 1.8 \pm 0.4$  should match  $\alpha_r$  for iC-CMB, which it does not ( $\alpha_r \approx 0.65$  to  $0.68$  over

the brightest regions of the radio lobes). Moreover, we have modelled the brightest parts of each radio lobe as spheres of radii 8 arcsec, and found minimum-energy magnetic fields (without protons) of 1.5 and 1.4 nT for the S and N lobes, respectively<sup>3</sup>. With these field strengths, only about 5 percent of the 1-keV flux density of extended emission is accommodated, and the field would need to be reduced by a factor of about 6 for iC-CMB emission to be at a level comparable to the X-ray emission seen. This factor is much larger than typical of radio lobes (Croston et al. 2005). Even then the steep spectrum would still not be explained, and so we consider non-thermal explanations for the extended X-ray emission no further.

## 4 DISCUSSION

### 4.1 Large-scale gas

We have argued that the extended X-ray emission is dominated by emission from gas of  $kT \approx 1$  keV, a temperature appropriate for group gas. The inferred bolometric luminosity in a source-centre annulus of radii 6 and 25 arcsec is  $L_{\text{bol}} = 3.6 \times 10^{41}$  ergs s<sup>-1</sup> (or  $L_x = 2.7 \times 10^{41}$  ergs s<sup>-1</sup> in the commonly-used 0.1-2.4 keV band). To test roughly if the surface brightness lends support for a group origin, we have fitted a  $\beta$ -model to a radial profile of the emission within this annulus. The best fit gives  $\beta = 0.42$  and a core radius of 7.3 arcsec, although uncertainties are large. Based on scaling relations of Vikhlinin et al. (2006) it is necessary for this system to go out to a radius of roughly 295 arcsec to reach  $r_{500}$ . If we then restrict  $\beta$  to lie in a reasonable range of 0.4–0.6, we find an extrapolated  $L_{\text{bol}}(L_x)$  within  $r_{500}$  of  $2.5^{+1.0}_{-1.7}(1.9^{+0.8}_{-1.3}) \times 10^{42}$  ergs s<sup>-1</sup>, which is not unreasonable for a group atmosphere of this temperature (see e.g., Lovisari, Reiprich & Schellenberger 2015). However, it is striking that the detected X-ray emission covers only the radio lobes.

How recently the group was formed is an interesting question. The NASA Extragalactic Database (NED) reveals the presence of several fainter galaxies within a projected radius of 120 kpc (75 arcsec) of 3C 277.3. While velocity data are largely lacking, 2MASX J12541671+2736531, with an appearance in *HST* data of an edge-on spiral, lies on the perimeter of such a circle and is separated in velocity by only about 600 km s<sup>-1</sup>. Thus it is reasonable to suppose the presence of group companions. The evidence for 3C 277.3 expanding into at least  $10^9$  M<sub>⊙</sub> of relatively settled gas covering the lobes led Morganti et al. (2002) to propose that a major merger commenced at least  $10^8$  years ago, before the triggering of the radio source. We estimate the mass in X-ray-emitting gas to be roughly  $10^{11}$  M<sub>⊙</sub> within a radius of 25 arcsec of the centre. This then dominates the mass of the presumed merger remnant, and argues that the group atmosphere is likely to pre-date the merger.

The morphological comparison between the radio and X-ray emission (Section 3.1) shows evidence for the radio lobes having bored cavities in the gas, as is found common

<sup>3</sup> Field strengths published by van Breugel et al. (1985) are slightly higher. This is as expected since protons of equal energy to the electrons were used in those calculations.

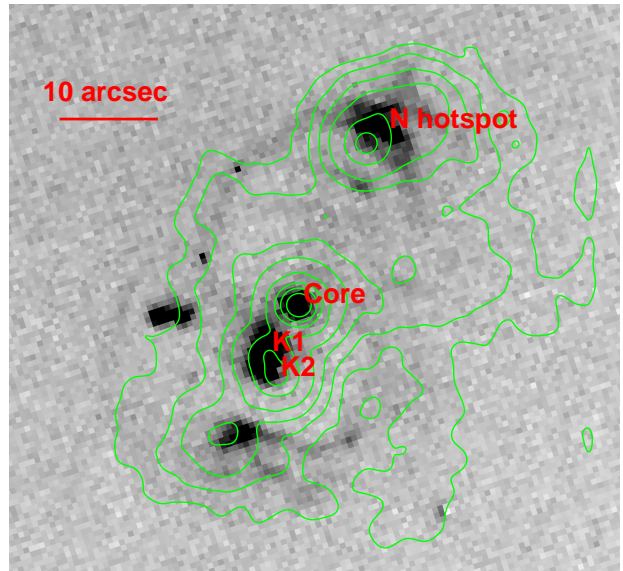


**Figure 7.** X-ray contours (from the image of Figure 3) on the H $\alpha$  image from figure 1b of Tadhunter et al. (2000).

in group and cluster atmospheres (e.g., Panagoulia et al. 2014). In group atmospheres cavities are found to be accompanied by particularly strong shocks, with Mach numbers ranging from about 1.5 to 3, such as in HCG 62 (Gitti et al. 2010), NGC 5813 (Randall et al. 2011) and PKS B2152-699 (Worrall et al. 2012), although only in the last case is the radio source from the FRI/II class of which 3C 277.3 is also a member and which is expected to be most characteristic of heating in the Universe as a whole. The way in which the X-ray enhancements embrace the radio lobes of 3C 277.3 points to relatively strong shocks being likely here too, although the X-ray emission is too weak for quantitative assessment of shock speed.

Worrall et al. (2012) found for PKS B2152-699 that the the cavity power,  $P_{\text{cav}}$ , increased by a factor of 40 once the deduced Mach number ( $\approx 3$ ) of the expansion and the kinetic and thermal energy in shocked gas are taken into account. Without this increase,  $P_{\text{cav}}$  was much too low to fall on an extension from FRI to FRI/II powers of correlations with 1.4-GHz radio power (Cavagnolo et al. 2010). For 3C 277.3 we cannot measure a Mach number for the expansion, but we do find that  $P_{\text{cav}}$  falls far below correlations unless there is a significant energy contribution from strong shocks. The total 1.4-GHz flux density from the NVSS survey (Condon et al. 1998) is 2.9 Jy, leading to  $P_{1.4} \approx 7 \times 10^{41}$  erg s<sup>-1</sup> and an expected cavity power from correlations of  $P_{\text{cav}}$  of  $2 \times 10^{45}$  erg s<sup>-1</sup>, although with large errors (Cavagnolo et al. 2010). In contrast, assuming the group gas in a sphere of radius 7'' has been pushed aside by each lobe in a lifetime of about 10 Myr (see Section 4.2, a factor of four shorter than the sound-crossing time in the group gas), with no correction for the kinetic and thermal energy in shocked gas we estimate a cavity power of only  $P_{\text{cav}} \approx 3 \times 10^{43}$  erg s<sup>-1</sup>.

The argument that the observed X-ray gas is shocked by the radio lobes of 3C 277.3 is also supported by a morpholog-



ical comparison between the locations of X-ray and cooler gas around the lobes. While the picture of enhancements embracing the radio lobes is generally similar to that seen in  $H\alpha$ , an overlay of X-ray contours on an emission-line image (Figure 7) suggests that, with the exception of the core, jet-cloud interaction region and northern hotspot, there is an anti-correlation of X-ray and  $H\alpha$  emission, particularly for filaments of emission-line gas in the east and south-west quadrants. This can be understood if shock advance around the lobe is responsible for the X-ray brightening, and is inhibited by denser  $H\alpha$ -emitting material. The anti-correlation is not easy to understand if the lobes are weakly pushing aside the external medium, since in that case X-ray and  $H\alpha$  co-location would not be disfavoured.

The combined result of the arguments above is that the lobe expansion of 3C 277.3 is likely to be similar to that of the jet-cloud-interacting FRI/II source PKS B2152-699. In both cases the time averaged jet power imparted to pre-existing group gas is primarily in the form of kinetic and thermal energy of shocked gas.

#### 4.2 Jet-interaction region

The eastern displacement with respect to the radio of the X-rays associated with K1 is what is expected if we are seeing hot gas associated with the cloud of previously-known, cooler, optical emission-line gas. The emission-line cloud was first reported by Miley et al. (1981). It was explored further by van Breugel et al. (1985) who found a mass<sup>4</sup> of about  $4 \times 10^6 M_\odot$ , and argued on energetic grounds that it was local gas that is being heated and entrained by the jet rather than having been transported from the nucleus. The X-ray detection makes that conclusion even more solid, since the cloud mass grows by more than an order of magnitude once the mass of the X-ray-emitting envelope is taken into account (see below). The required spatial resolution for improved mapping of the morphology of the optical gas became available with *HST*, and Martel et al. (1999) commented on the cloud's north-south orientation and filamentary appearance based on 1995 observations using the F702W filter [see also Capetti et al. (2000) who incorporated F555 data]. In Figure 8 we show archival *HST* continuum data from 1997 alongside an X-ray image. In Figure 9, X-ray contours are overlaid on a continuum-subtracted narrow-band *HST* image centered on the [O III] emission line. Despite the poorer X-ray resolution, the association between the X-ray and optical emission is clear. These emissions are adjacent to, rather than coincident with, the radio peak at K1.

We estimate the physical properties of the X-ray gas associated with the K1 gas cloud assuming the emission fills a sphere of radius 1.1 arcsec (diameter 3.5 kpc) with uniform density, using equations from section 4.4 of Worrall et al. (2012). We find a density of hydrogen nuclei  $n_p = 2_{-1.5}^{+0.5} \times 10^5 \text{ m}^{-3}$ , a pressure of  $P = 3_{-1.6}^{+4} \times 10^{-11} \text{ Pa}$ , and a total X-ray gas mass of  $M_{\text{Xgas}} = 17_{-13}^{+4} \times 10^7 M_\odot$ . If the X-ray gas is not still heated, e.g., by the radio jet, the cooling time is  $60_{-20}^{+120} \text{ Myr}$ . The average pressure in the group X-ray gas is found to be roughly 10 and  $4 \times 10^{-13} \text{ Pa}$  at radii of 10 and 25 arcsec, respectively. At a radius of 6 arcsec, comparable to that of

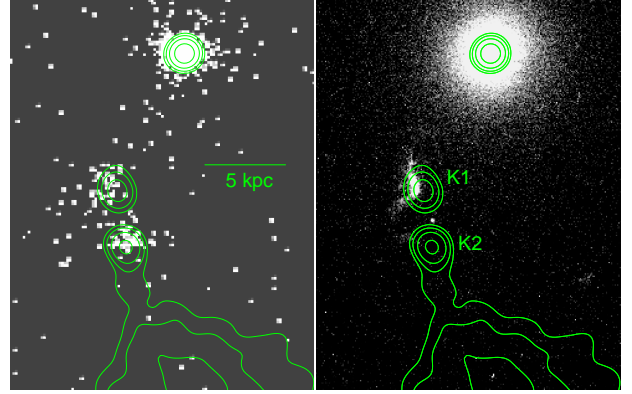


**Figure 8.** X-ray emission in K1 (left panel, data from Figure 2) is offset relative to the radio contours in the same sense as are the optical filaments (right panel, *HST* WFPC2 F555W image formed from archival datasets u3a12z01t and u3a12z02t).

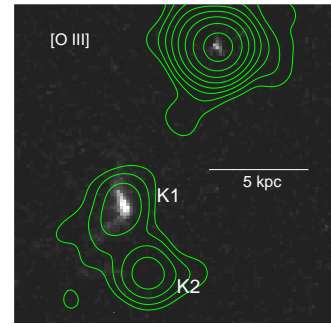


**Figure 9.** X-ray contours (lowest of  $3\sigma$  significance) on an *HST* [O III] image formed from subtracting a scaled version of an image in F555W from that in FR533N. Note the X-ray and [O III] align well at K1 and the nucleus.

the K1 gas cloud we find  $1.5_{-0.4}^{+0.3} \times 10^{-12} \text{ Pa}$ . The group gas cannot therefore contain the gas cloud, which should expand and dissipate in the sound crossing time of about 10 Myr. We infer that the cloud was originally cooler material that has been heated to X-ray temperatures within the lifetime of the radio source due to the passage of the jet.

We note that the X-ray properties of the gas cloud are not dissimilar to those found in the closer, and so brighter and better constrained, high ionization cloud (HIC) interacting with the jet in PKS B2152-699. Indeed, for PKS B2152-699's HIC,  $P \approx 8 \times 10^{-11} \text{ Pa}$ ,  $M_{\text{Xgas}} \approx 7 \times 10^7 M_\odot$ ,  $kT \approx 0.3 \text{ keV}$ , and the gas cloud was heated within the lifetime of the radio source (Worrall et al. 2012). Differently from PKS B2152-699, in the HIC of 3C 277.3 the optical emission lines are narrow and in a high ionization state, with a total flux in [O III] of  $3 \times 10^{-14} \text{ ergs cm}^{-2} \text{ s}^{-1}$  (Solórzano-Iñarrea & Tadhunter 2003). The narrowness of the lines was unexpected because the jet-cloud interaction appears to be strong, but one of the possible explanations proffered by Solórzano-Iñarrea & Tadhunter (2003) is supported by our detection of X-rays associated with the cloud. The idea is that the optical emission-line gas is not itself shocked, but lies around the shocked structures, and

<sup>4</sup> scaled up by a factor of two following note added in proof.



is photoionized by photons emitted by gas behind the shock front. The [O III] line luminosity is high, at  $5 \times 10^{41}$  ergs  $\text{s}^{-1}$ , but the X-ray luminosity (extrapolated from the fitted parameter values to include all photons above 13.6 eV), at  $2.4_{-1.5}^{+6.5} \times 10^{41}$  ergs  $\text{s}^{-1}$ , can provide a significant fraction of the required photoionizing power. The gas that is shocked by interaction with the radio jet is likely to be structurally complex, and lower-temperature components (e.g., in the ultraviolet) could plausibly make up any deficit.

The isotropic X-ray luminosity of the nucleus is about  $2 \times 10^{43}$  ergs  $\text{s}^{-1}$ , after correction for the high absorption (Section 3.2). If the nuclear X-ray spectrum extends to high energy without downwards curvature, this would be an underestimate. The cloud could intercept about 1 per cent of this luminosity, and so the contribution of ionizing photons from the nucleus will be similar to, or could exceed, the contribution from the X-ray-bright gas at K1. We note that Ramírez et al. (2014) contradicts the high polarization at K1 reported by Miley et al. (1981), and so there is no evidence that the optical continuum at K1 arises from scattered nuclear light.

We have found above that the X-ray gas cloud can be no older than 10 Myr. It is then interesting to attempt to relate this to the likely age of the radio source. From Figure 1 we see that the southern lobe is morphologically consistent with plasma originating from a jet travelling from K1 to K2, rather than from an historically un-deflected jet. Although we note that both lobes show more distortion on the east than west, the side on which more of the H $\alpha$ -emitting filaments mapped by Tadhunter et al. (2000) lie, it seems more plausible that the southern jet was bent early on in the lifetime of the source than being a late-phase re-direction. This makes 3C 277.3 no older than about 10 Myr. Such an age fits with the source's relatively small projected linear size and our argument (unlike for PKS B2152-699 which is of similar projected size) that it lies close to the plane of the sky, and so is of relatively small intrinsic size.

The nature of the jet-cloud interaction will be explored further using new Integral Field Unit data from Gemini North (Duncan Smith et al, work in progress).

### 4.3 Nonthermal X-ray components

The X-ray emission associated with K2 peaks upstream of the radio. This has been seen elsewhere in X-ray synchrotron knots embedded in the jets of nearby radio galaxies, most notably in 3C 66B, Cen A, 3C 346, 3C 353 and possibly 3C 15 (Hardcastle, Birkinshaw & Worrall 2001; Hardcastle et al. 2003; Worrall & Birkinshaw 2005; Kataoka et al. 2008; Dulwich et al. 2007). The spectral constraint on the X-ray emission from knot K2 is rather poor and alone does not rule out an origin as either inverse Compton emission from electrons of energies similar to those producing the radio synchrotron emission, or synchrotron radiation from high-energy electrons of steeper spectrum. The deflection at K1 has been interpreted by Tingay (1977) in the context of an oblique-shock model to support a pre-shock jet Lorentz factor of between 3 and 5, a post-shock Lorentz factor of between 1.1 and 1.5, and a jet orientation of less than 75 degrees to the line of sight. Even if the post-shock orientation angle is as small as a few degrees (unlikely due to the X-ray absorption against the nucleus, Section 3.2), the Doppler fac-

tor in K2 will be insufficient to produce the X-ray emission through boosting of inverse-Compton scattered photons, as may be important in quasar jets (see e.g., Worrall 2009; Marshall et al. 2011, and references therein). For negligible beaming, predictions for synchrotron self-Compton emission and Compton scattering of CMB photons, based on a minimum-energy magnetic field, fall short of observations by factors of roughly 1300 and 600, respectively. However, K2 is only 13 kpc from the nucleus, and starlight will provide additional photons. To estimate their contribution we have assumed the host galaxy to have similar properties to that for PKS B2152-699, for which we modelled the local energy density of starlight as a function of position (Worrall et al. 2012). We find an X-ray contribution that is roughly five times the contribution from unscattered CMB radiation – still far below what is required.

We therefore conclude that the X-ray emission in K2 is dominated by synchrotron radiation. This is the established mechanism for X-rays from FRI radio galaxies (Worrall, Birkinshaw & Hardcastle 2001; Harwood & Hardcastle 2012). It was first claimed in knots of specific FR II radio galaxies by Wilson, Young & Shopbell (2001); Worrall & Birkinshaw (2005); Kraft et al. (2005); Kataoka et al. (2008), and is studied in detail in the bright jet of Pictor A (Hardcastle et al. 2015). X-ray synchrotron jet emission is also seen in the FRI/II transition source PKS B2152-699 (Worrall et al. 2012), where as in 3C 277.3,  $\alpha_{\text{rx}} \approx 1$ .

Bright nonthermal X-rays on the upstream edge of a radio hotspot (Sections 3.1 and 3.3) have been noted previously in other sources (e.g., Erlund et al. 2007; Hardcastle, Croston & Kraft 2007), with a variety of suggested explanations. Indeed an offset is seen in PKS B2152-699, but with the main difference that the offset in that source is for the hotspot on the jet-side of the source, approaching at small angle to the line of sight. Following Georganopoulos & Kazanas (2003), Worrall et al. (2012) argue that inverse-Compton scattering of hotspot synchrotron emission by the approaching jet may provide an explanation for that offset. 3C 277.3 has only one (N) radio hotspot, but as it is on the side of the source highly unlikely to be approaching the observer, a different explanation must apply.

At 0.4-arcsec resolution the radio map of the N hotspot starts to break into faint radio substructure. Tingay et al. (2008) have suggested, based on VLBI imaging principally of Pictor A, that variable pc-scale regions host strong shocks that accelerate electrons to TeV energies and give significant X-ray synchrotron emission. This may be happening in 3C 277.3. In a minimum-energy magnetic field it would take the whole flux density of the hotspot (about 113 mJy at 4.9 GHz) in a pc-scale region to produce the X-rays via the synchrotron self-Compton mechanism. Instead, overlooking the non-contemporaneous nature of the radio and X-ray data, at most 3 mJy of radio flux density comes from the X-ray-bright region, but this implies  $\alpha_{\text{rx}} \approx 0.9$ , which is similar to the value of  $\alpha_{\text{rx}}$  in K2 for which we have argued a synchrotron origin. Unfortunately the hotspot X-rays are too faint for us to comment on possible variability between the 2010 and 2014 data, which might address the issue of source size, but more sensitive high-resolution radio mapping closer in date to the X-ray observations could help explore the likely synchrotron origin further.

## 5 SUMMARY AND CONCLUSIONS

The radio galaxy 3C 277.3 is an ideal test-bed for studying the energy deposition of a radio galaxy typical of those dominating radio-mode feedback in the wider Universe, since it has typical power and resides in a typical (group) environment. Remnants of cold and excited gas from the merger that probably triggered the radio outburst have previously been studied dynamically through their line emission. In this paper we have reported the discovery with *Chandra* of X-ray-emitting gas dominating the baryonic mass of the system both on the group scale and in the jet-cloud interaction region that is responsible for having bent the jet by a projected angle of  $40^\circ$ . Our primary conclusions can be summarized as follows:

(i) The expanding radio galaxy has been responsible for shocking a pre-existing X-ray group atmosphere which now, to some extent, embraces the lobes. We estimate the mass of group gas out to a radius of 40 kpc as  $10^{11} M_\odot$ . Shock advance in some places is inhibited by the cold merger material. The kinetic and thermal energy of shocked gas then dominates the overall heat input from the radio galaxy to the external medium.

(ii) The emission-line cloud responsible for bending the jet is dominated by X-ray gas of mass about  $2 \times 10^8 M_\odot$ . The X-ray spectrum of the nucleus contains a highly absorbed component arguing that the galaxy lies close to the plane of the sky. The large projected jet bend is then also a large intrinsic bend.

(iii) The emission-line cloud can be no older than 10 Myr or it should have expanded away. The fact that the radio lobe (containing old jet material) is inflated around the post-bend jet direction allows us to date the whole radio source as no older than 10 Myr.

(iv) The discovery of dominant X-ray-radiating gas associated with the emission-line cloud goes some way to solving the mystery of the narrowness of the optical emission lines in the cloud. The X-ray material can provide about  $2 \times 10^{41} \text{ ergs s}^{-1}$  to photoionize the cloud, suggesting the optical emission-line gas may be unshocked. Ionizing continuum from the core could provide a similar level of excitation at the cloud.

(v) X-ray emission is detected from the southern jet and northern hotspot, in both cases offset upstream from radio peaks. We argue that in both cases the X-ray emission is likely to be synchrotron radiation.

The closer source PKS B2152-699 shares many of the properties of 3C 277.3, such as typical radio power, shocked group atmosphere, and is also further enriched by revealing a jet-cloud interaction region. As compared with 3C 277.3, the radio outburst of PKS B2152-699 is estimated to be somewhat older, there is no longer evidence of large-scale merger gas (if indeed it existed), and the jet-cloud interaction may be younger and more localized, with the jet having multiply scarred the cloud with which it is interacting. Both sources have grown into the plateau stage where they are expected to spend most of their lives, and so can be considered as touchstones for revealing how typical radio-mode heating may occur in the Universe.

## ACKNOWLEDGMENTS

We thank Clive Tadhunter for providing the  $H\alpha$  data from Tadhunter et al. (2000) that we use in Figure 7. We acknowledge support from NASA grant GO3-14118X. Results are largely based on observations with *Chandra*, supported by the CXC. The National Radio Astronomy Observatory is a facility of the National Science Foundation operated under cooperative agreement by Associated Universities, Inc. This research has made use of the NASA/IPAC Extragalactic Database (NED) which is operated by the Jet Propulsion Laboratory, California Institute of Technology, under contract with the National Aeronautics and Space Administration.

## REFERENCES

- Balmaverde et al., 2012, A&A, 545, A143
- Baum, S.A., Heckman, T., 1989, ApJ, 336, 702
- Best et al. 2005 MNRAS 362, 9
- Bridle, A.H., Fomalont, E.B., Palimaka, J.J., Willis, A.G., 1981, ApJ, 248, 499
- Buttiglione, S., Capetti, A., Celotti, A., Axon, D.J., Chiaberge, M., Macchetto, F.D., Sparks, W.B., A&A, 2009, 495, 1033
- Buttiglione, S., Capetti, A., Celotti, A., Axon, D.J., Chiaberge, M., Macchetto, F.D., Sparks, W.B., A&A, 2010, 509, A6
- Capetti, A., de Ruiter, H.R., Fanti, R., Morganti, R., Parma, P., Ulrich, M.-H., 2000, A&A, 362, 871
- Capetti, A., Celotti, A., Chiaberge, M., de Ruiter, H.R., Fanti, R., Morganti, R., Parma, P., 2002, A&A, 383, 104
- Cavagnolo, K.W., McNamara, B.R., Nulsen, P.E.J., Carilli, C.L., Jones, C., Birzan, L., 2010, ApJ, 720, 1066
- Churazov, E., Gilfanov, M., Forman, W., Jones, C., 1996, ApJ, 471, 673
- Condon, J.J., Cotton, W.D., Greisen, E.W., Yin, Q.F., Perley, R.A., Taylor, G.B., Broderick, J.J., 1998, ApJ, 115, 1693
- Croston, J.H., Hardcastle, M.J., Harris, D.E., Belsole, E., Birkinshaw, M., Worrall, D.M., 2005, ApJ, 626, 733
- Dickey, J.M., Lockman, F.J., 1990, ARA&A, 28, 215
- Done, C., Magdziarz, P., 1998, MNRAS, 298, 737
- Dulwich, F., Worrall, D.M., Birkinshaw, M., Padgett, C.A., Perlman, E.S., 2007, MNRAS, 374, 1216
- Erlund, M.C., Fabian, A.C., Blundell, K.M., Moss, C., Ballantyne, D.R., 2007, MNRAS, 379, 498
- Evans, D.A., Worrall, D.M., Hardcastle, M.J., Kraft, R.P., Birkinshaw, M., 2006, ApJ, 642, 96
- Georganopoulos, M., Kazanas, D., 2003, ApJ, 589, L5
- Gitti, M., O'Sullivan, E., Giancintucci, S., David, L.P., Vritilek, J., Raychaudhury, S., Nulsen, P.E.J., 2010, ApJ, 714, 758
- Hardcastle, M.J., Birkinshaw, M., Worrall, D.M., 2001, MNRAS, 326, 1499
- Hardcastle, M.J., Worrall, D.M., Kraft, R.P., Forman, W.R., Jones, C., Murray, S.S., 2003, ApJ, 593, 169
- Hardcastle, M.J., Croston, J.H., Kraft, R.P., 2007, ApJ, 669, 893
- Hardcastle, M.J. et al, 2015, MNRAS, in press
- Harwood, J.J., Hardcastle, M.J., 2012, MNRAS, 423, 1368
- Kataoka, J. et al., 2008, ApJ, 584, 839
- Kim, D.-W., Fabbiano, G., 2004, ApJ, 611, 846
- Kraft, R.P., Hardcastle, M.J., Worrall, D.M., Murray, S.S., 2005, ApJ, 622, 149
- Lovisari, L., Reiprich, T.H., Schellenberger, G., 2015, A&A, 573, A188
- Ly, C., De Young, D.S., Bechtold, J., 2005, ApJ, 619, 609
- Marshall, H.L., et al., 2011, ApJS, 193, 15
- Martel, A.R. et al., 1999, ApJS, 122, 81
- McNamara, B.R., Nulsen, P.E.J., 2012, New J. Phys, 14, 055023

- Miley, G.K., Heckman, T.M., Butcher, H.R., van Breugel, W.J.M., 1981, *ApJ*, 247, L5
- Morganti, R., Oosterloo, T.A., Tinti, S., Tadhunter, C.N., Wills, K.A., van Moorsel, G., 2002, *A&A*, 387, 830
- Panagoulia, E.K., Fabian, A.C., Snaders, J.S., Hlavacek-Larrondo, J., 2014, *MNRAS*, 444, 1236
- Ramírez, E.A., Tadhunter, C.N., Axon, D., Batcheldor, D., Packham, C., Lopez-Rodriguez, E., Sparks, W., Young, S., 2014, *MNRAS*, 444, 466
- Randall, S.W. et al., 2011, *ApJ*, 726, 86
- Rines, K., Geller, M.J., Kurtz, M.J., Diaferio, A., Jarrett, T.H., Huchra, J.P., 2001, *ApJ*, 561, L41
- Solórzano-Iñarra, C., Tadhunter, C.N., 2003, *MNRAS*, 340, 705
- Tadhunter, C.N., Villar-Martin, M., Morganti, R., Bland-Hawthorn, J., Axon, D., 2000, *MNRAS*, 314, 849
- Tilak, A., O’Dea, C.P., Tadhunter, C., Wills, K., Morganti, R., Baum, S.A., Koekemoer, A.M., Dallacasa, D., 2005, *AJ*, 130, 2513
- Tingay, S.J., 1997, *A&A*, 327, 550
- Tingay, S.J., Lenc, E., Brunetti, G., Bondi, M., 2008, *AJ*, 136, 2473
- Urry, C.M., Padovani, P., 1995, *PASP*, 107, 803
- van Breugel, W., Miley, G., Heckman, T., Butcher, H., Bridle, A., 1985, *ApJ*, 290, 496
- Vikhlinin, A., Kratsov, A., Forman, W., Jones, C., Markevitch, M., Murray, S.S., & Van Speybroeck, L. 2006, *ApJ*, 640, 691
- Wilson, A.S., Young, A.J., Shopbell, P.L., 2001, *ApJ*, 547, 740
- Worrall, D.M., 2009, *A&ARv*, 17, 1
- Worrall, D.M., Birkinshaw, M., 2005, *MNRAS*, 360, 926
- Worrall, D.M., Birkinshaw, M., 2014, *ApJ*, 784, 36
- Worrall, D.M., Birkinshaw, M., Hardcastle, M.J., 2001, *MNRAS*, 326, L7
- Worrall D.M., Birkinshaw, M., Young, A.J., Momtahan, K., Fosbury, R.A.E., Morganti, R., Tadhunter, C.N., Verdoes Kleijn, G., 2012, *MNRAS*, 424, 1346
- Young, A.J., Wilson, A.S., Tingay, S.J., Heinz, S., 2005, *ApJ*, 622, 830